Journal of Hydrology 607 (2022) 127501

Contents lists available at ScienceDirect

Journal of Hydrology

journal homepage: www.elsevier.com/locate/jhydrol

Research papers

Physical vulnerability to dynamic flooding: Vulnerability curves and vulnerability indices

Maria Papathoma-Köhle [a,*], Matthias Schlögl [a], Lea Dosser [a], Florian Roesch [a], Marco Borga [b], Marcel Erlicher [b], Margreth Keiler [c,d], Sven Fuchs [a]

[a] University of Natural Resources and Life Sciences, Department of Civil Engineering and Natural Hazards, Institute of Mountain Risk Engineering, Peter-Jordan-Strasse 82, 1190 Vienna, Austria
[b] University of Padova, Department of Land, Environment, Agriculture and Forestry, Viale Dell'Universita', 16, 35020 Legnaro, Italy
[c] University of Innsbruck, Department of Geography, Innrain 52f, 6020 Innsbruck, Austria
[d] Austrian Academy of Sciences, Institute for Interdisciplinary Mountain Research, Innrain 25/3, 6020 Innsbruck, Austria

ARTICLE INFO

This manuscript was handled by Emmanouil Anagnostou, Editor-in-Chief

Keywords:
Dynamic flooding
Vulnerability curves
Vulnerability indices
Degree of loss
European Alps

ABSTRACT

Vulnerability analysis is crucial to assess natural hazard risk. Methods for vulnerability assessment include indices as well as vulnerability curves. Vulnerability curves make use of empirical data to show the relationship between the process intensity and the resulting degree of loss on each affected building whereas vulnerability indices are based on a number of indicators representing building characteristics and their surroundings. In the present paper, damage data from two relatively recent torrential events in the European Alps are used to compare results using a vulnerability curve (Beta model) and a physical vulnerability index (PVI). Following the application of both methods, their strengths and weaknesses are outlined. Vulnerability curves constitute a valuable quantitative method for the assessment of physical vulnerability but, in the present study, they tend to overestimate damages. On the other hand, vulnerability indices better support the understanding of local-scale damage patterns but they require detailed data and further research on weighting and indicator selection. The study leads to the conclusion that both methods complement each other providing better insights into the physical vulnerability of buildings exposed to torrential hazards. Furthermore, uncertainties associated with the two approaches are related to the required data. Therefore, a sensitivity analysis is carried out showing that process intensity is a key variable for the assessment of vulnerability, whereas, differences in the calculation of the degree of loss based on different building values are less important. Finally, the paper gives clear recommendations for improved event and damage documentation and provides an outlook on future needs in vulnerability assessment, including constant updating of both methods based on recent events.

1. Introduction

Mountain rivers are characterized by flow patterns with variable amounts of sediment erosion, deposition, and remobilisation (Borga et al., 2014; Church and Jakob, 2020; Sturm et al., 2018b) that are hereinafter referred to as dynamic flooding. Typical hazard processes associated with dynamic flooding include fluvial sediment transport, debris flows, and related phenomena (Karagiorgos et al., 2016; Mazzorana et al., 2014; Milanesi et al., 2018; Slaymaker, 2010). Dynamic flooding events may not affect large areas the way river floods or earthquakes do but they cause significant interruption and monetary damage to households and the local community (Fuchs et al., 2015; Schlögl et al., 2019; Zhang et al., 2018; Zischg et al., 2018; Zou et al., 2018).

Analysis, assessment, and visualisation of vulnerabilities can provide the basis for the development of mitigation or adaptation strategies aiming to reduce the consequences of natural hazards. Physical vulnerability in particular is directly connected to monetary loss and interruptions that are in the centre of the interests of several stakeholders including governments, authorities, insurance companies, engineers, and homeowners. For this reason, several approaches have been developed over the years for the assessment of physical vulnerability (Vamvatsikos et al., 2010; Fuchs et al., 2019b). A review of methods used for the assessment of the physical vulnerability of buildings to

* Corresponding author.
E-mail address: maria.papathoma-koehle@boku.ac.at (M. Papathoma-Köhle).

https://doi.org/10.1016/j.jhydrol.2022.127501
Received 1 December 2021; Received in revised form 15 January 2022; Accepted 18 January 2022
Available online 29 January 2022

dynamic flooding suggests that there are mainly three methods used: vulnerability matrices, curves (or functions) and indices (Papathoma-Köhle et al., 2017). According to this review, the most common method is the vulnerability curves. Built on empirical data, vulnerability curves are based on the assessment of observed damage linked to underlying process intensities (Fuchs et al., 2007). Consequently, vulnerability ranges from 0 (no damage) to 1 (complete destruction). They are important because they can also be used to compute the expected monetary loss of specific future scenarios and, for this reason, they constitute a valuable tool for planners, engineers, and local authorities (Fuchs et al., 2019a; Sturm et al., 2018a).

Nevertheless, two main drawbacks have been identified with respect to vulnerability curves. Firstly, the spread of loss data is high so that the resulting vulnerability curves are often only used to show the expected mean loss associated with specific process intensities. Secondly, input data are related to economic variables, such as the loss and the reconstruction value of affected buildings, and other characteristics of affected buildings that influence the loss are only indirectly acknowledged in the overall assessment. These characteristics, however, play often a pivotal role in the question of whether or not damage occurs (Mazzorana et al., 2014; Sturm et al., 2018a), and include information on the building design and the overall location of the building towards the hazard process. Therefore, an alternative method to assess vulnerability that considers building characteristics has been considered necessary (Papathoma-Köhle et al., 2019).

Vulnerability indices have been presented as an alternative method (Fuchs et al., 2019b). These indices consider building characteristics and once they are identified and quantified with respect to their impact on triggering damage, they can be used to assess vulnerability without requiring empirical damage data from past events (Papathoma-Köhle et al., 2019). Although such indices have their roots in social vulnerability assessment (for an overview, see e.g. Cutter and Finch, 2008; Fekete, 2019), they also were increasingly used for the assessment of physical vulnerability. However, similar to the use of vulnerability curves, some inherent uncertainties make their application challenging, especially in data-scarce regions as illustrated by Malgwi et al. (2020) and Malgwi et al. (2021). Additionally, these challenges are related to the lack of studies focusing on the validation of existing indices or sensitivity analysis of existing indicators (Chow et al. 2019; Agliata et al., 2021; Moreira et al., 2021). The aim of the present paper is to close this gap and to contribute to the ongoing discussion in mountain hazard risk management. Starting with a current model to assess physical vulnerability using a curve (Beta model), we present the challenges that arise when this model is applied to two recent incidents that occurred in the Italian and Austrian Alps. These events have been chosen due to the nature of the natural process (dynamic flooding), the similarity of the building design to the buildings that have been used for the original Beta model and PVI, and the data availability. Furthermore, we apply in the same case study areas a physical vulnerability index (PVI) and we compare the results with the actual degree of loss. In this way, the predictive capacity of the vulnerability index can be assessed and its potential to supplement vulnerability curves is demonstrated. Additionally, a sensitivity analysis is carried out so that the dependency of the overall index on the target variables becomes evident. The results of the sensitivity analysis may be used to inform damage documentation practices to make them more accurate and precise. The authors have used empirical data to develop the specific tools (vulnerability curve and vulnerability index) in previous studies (Fuchs et al., 2019a, Papathoma-Köhle et al., 2019) and this is the first time that both tools will be applied in newly derived empirical data from two recent events. Preliminary versions of the tools have been compared in the past (Papathoma-Köhle, 2016) leaving many possibilities for further development and setting the scene for the present paper.

2. Methods

In the following paragraphs, a brief overview of the general methods used to derive (a) the vulnerability curve and (b) the vulnerability index is provided.

2.1. Vulnerability curves

Vulnerability curves are used to link the process intensity affecting a building to the degree of loss (Arrighi et al., 2020; Englhardt et al., 2019; Fuchs et al., 2019a), whereas the latter is usually expressed in terms of a quotient between the replacement value of an individual building and the loss that was reported during a specific event (Fuchs et al., 2007). As far as the process intensity is concerned, it is proxied by the deposit height. This value is assessed by photographic documentation of the event or fieldwork by observing the mark of water and debris that has been left on the outside walls of a building. When the building is not located on flat ground the maximum (observed) or average (when the observations from all sides of the building are inspected) deposit height is considered. We use the word "intensity" and not "magnitude" because the value concerns a property of the process which is relevant to the element at risk (debris height on the building envelope).

It is clear from the literature, that there are more properties of the process that may influence its impact on a building other than the deposit height, including the velocity of the flow, its viscosity, and impact pressure (Quan Luna et al., 2011). Nevertheless, these properties are usually not captured during an event by e.g. measurements, but have to be modelled with resulting uncertainties of verification and validation respectively (Fuchs et al., 2019b). In summary, the variables used for the development of the vulnerability curves include:

1. The process intensity (proxied by the deposit height)
2. The degree of loss (DoL): expressed as the ratio of the building value lost. The degree of loss can be calculated when the following variables are known:
   a. The value of the building (as the reconstruction and not the market value which may depend on other factors such as proximity to infrastructure, touristic location, view).
   b. The monetary damage e.g. the compensation that the building owner received to rebuild or the monetary loss calculated by assessing the costs of partial damages and their repair.

As such, if the above information is available for a sufficient number of buildings, a model can be used to compute the resulting vulnerability curve (Fuchs et al., 2019a). This model includes the process intensity as the explaining variable and specifically supports the computation of mean losses for buildings affected by accounting for data skewness. Moreover, the model is an extension of classical empirical approaches that rely on a normal distribution of the degree of loss, and allows for an ex-ante assessment of damage once potential process intensities and the values of elements at risk are known (e.g. the studies of Cappabianca et al. (2008), Totschnig et al. (2011), Jakob et al. (2012), Cammerer et al. (2013), Totschnig and Fuchs (2013), etc.). One of these approaches especially developed for dynamic flooding is the zero-and-one-inflated Beta regression model (Fuchs et al., 2019a) in Fig. 1.

The model considers a large amount of data from recent events in the Eastern European Alps. Its solid predictive power warrants its application for supporting risk managers in the modelling of losses during different hazard scenarios and for different building types. The model shows clearly that the loss increases with increasing process intensity, proxied by deposition height. The loss increases rapidly once the deposition height of 1.5 m is exceeded which can be explained by the presence of windows that allow the flow to enter the building. The spread of the data for small intensities may be explained by the presence (in some cases) of a basement that despite the small intensity of the process increases the loss and the associated costs.

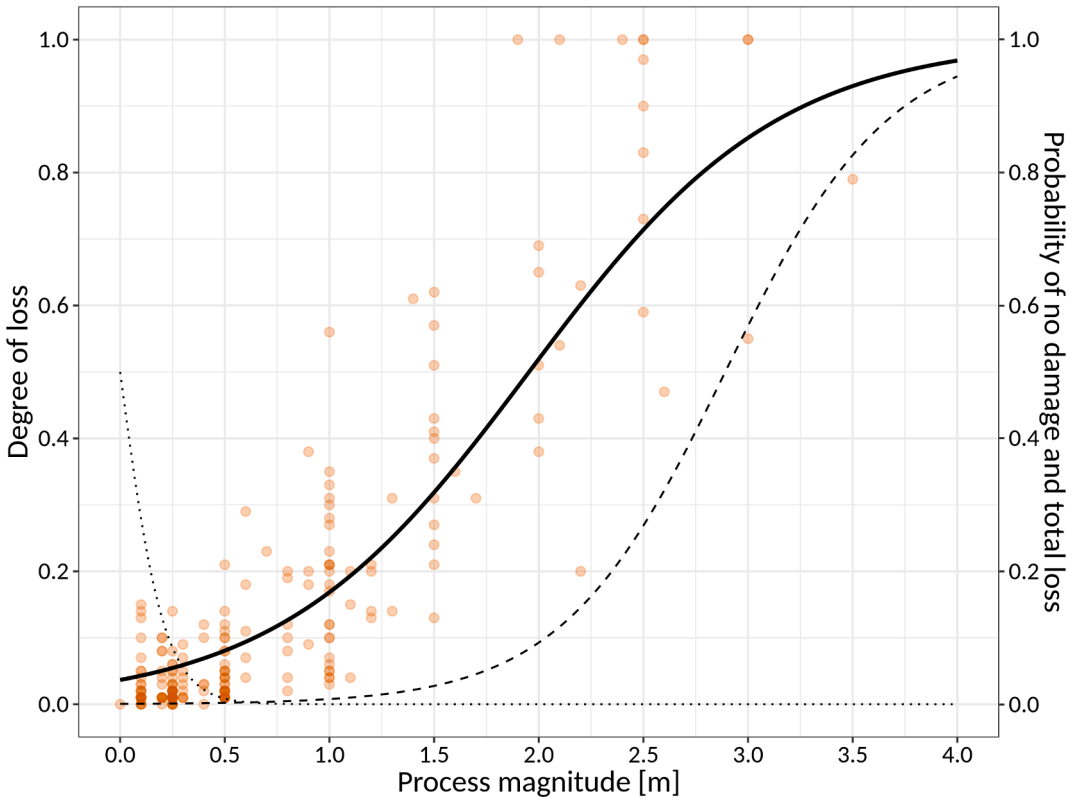

Fig. 1. The original zero-and-one-inflated Beta regression model. The dots represent the damaged buildings. The solid line shows the mean damage of the underlying Beta distribution as a result of different process intensities (deposit height). Additionally, the probability of an undamaged building is shown by the dotted line, and the probability of a building being completely damaged is shown by the dashed line (modified from Fuchs et al., 2019a).

2.2. The physical vulnerability index (PVI)

The Physical Vulnerability Index (PVI) for dynamic flooding has been developed based on the characteristics of buildings in the Austrian Alps that suffered significant damage during a dynamic flooding event in 2005 (Papathoma-Köhle et al., 2019). During the development of the approach, 23 indicators that were considered of being potentially important for explaining the degree of loss were collected for every building. These vulnerability indicators were winnowed by applying the all-relevant Boruta feature selection (Kursa and Rudnicki, 2010). The initial set of indicators included wall thickness, the existence of basement and basement openings, surrounding vegetation, ground slope, natural barriers, etc., however, the all-relevant Boruta feature selection revealed that only the following seven of these indicators proved to be able to explain the degree of loss:

- the exposure of the building expressed as the water level at the location of the building (*Ex*) (proxied by the process intensity),
- the vulnerability to water intrusion expressed as the number of levels affected by the flow (*WV*),
- the height of openings (windows) (H_{OP}),
- the height of the surrounding wall (SUR_{Wh}),
- the material of surrounding wall (SUR_{Wm}),
- the building row towards the flow (*ROW*), and
- the orientation of building (*ORI*).

The PVI was derived empirically by using the relative importance of each of the indicators as weight, resulting in the following equation:

$$PVI = (Ex \times 0.28) + (WV \times 0.23) + (H_{OP} \times 0.20) + (SUR_{Wh} \times 0.12) + (SUR_{Wm} \times 0.07) + (ROW \times 0.06) + (ORI \times 0.04) \quad (1)$$

The PVI was assigned to each building of the area under investigation and the spatial pattern of physical vulnerability was visualised in a map. The PVI can form the basis for decision-making as far as vulnerability reduction strategies are concerned including targeted building reinforcement, planning of structural protection measures, or recommending local adaptation measures.

The data requirements for the development of the PVI are considerably high. Detailed information on every building is required that in most of the cases can be acquired only following a detailed field survey. Nevertheless, some of the necessary information may be acquired by public authorities, photographic documentation, or online platforms such as Google Maps and Google Street View.

The main uncertainties associated with the development of PVI are related to data describing the vulnerability indicators as well as challenges in assessing the relevant process intensity on each building. Several uncertainties are associated with the intensity of the process (at least four out of seven indicators were related to the process intensity). Moreover, by validating the method on the basis of the actual degree of loss, different ways of calculating the value of buildings (and consequently the degree of loss) may influence the results of the validation.

2.3. Validation of the PVI and sensitivity analysis

To assess the validity of the PVI, the assigned PVI per building has been compared with the associated degree of loss, which is also an important input variable for the classical vulnerability curves. The degree of loss can be defined as the ratio of the building value that is lost following the impact of a natural process on a building. However, the degree of loss and its calculation are associated with a number of uncertainties. As far as the value of the buildings is concerned, it is important to clarify that this is not the market value, which may fluctuate due to location, view, touristic attractiveness, or proximity to infrastructure, but the amount of money needed to reconstruct the building (Fuchs and McAlpin, 2005). Data related to the consequences

(descriptive or monetary) of dynamic flooding events may be available by public authorities, may be acquired indirectly from photographic documentation, or may be provided by multiple sources leading to different results.

Furthermore, some of the indicators (e.g. height of openings and height of the surrounding wall) are directly related to the observed process intensity. Process intensity is often proxied by the deposition height (Fuchs et al., 2007; Totschnig and Fuchs, 2013), neglecting any other information on process intensities such as the flow velocity and pressure (Gall et al., 2009; Mazzorana et al., 2013; Milanesi et al., 2018; Sturm et al., 2018a; Chow et al. 2018). Information regarding the process intensity is usually collected also from photographic documentation (Papathoma-Köhle et al., 2012). Nevertheless, the assessment is not straightforward since in mountain environments buildings are often located on a slope, meaning that the deposition height may vary around the building (Fig. 2).

Thus, the main sources of uncertainty related to the required data for the application of a PVI and the sensitivity analysis can be summarized as follows:

1. Uncertainties related to the assessment of the process intensity: The process intensity (deposition height) per building is rarely quantified precisely and, as such, repeatedly mean or maximum values are used. In most cases, it is assessed from photographic documentation (Papathoma-Köhle et al., 2012; Totschnig et al., 2011), available video documentation (Milanesi et al., 2016) or it may be provided by modelling the process (Mazzorana et al., 2012; Quan Luna et al., 2011) or by civil protection authorities.
2. Uncertainties related to the monetary loss: The monetary loss per building is often provided by the authorities (compensation received per household owner) but, in some cases, it may not reflect the actual damage (see Holub and Fuchs (2009) and Thaler et al. (2018) for a discussion on loss compensation). An alternative way to acquire this information is by translating the actual damage seen in the photographic documentation to monetary units knowing the size of the building and the cost of the rehabilitation works (Papathoma-Köhle et al., 2012).
3. Uncertainties related to the value of the building: The value of the building may be acquired by multiple sources including insurance companies, authorities, tax offices etc. Differences in the calculation of the price derived from the way the size of the building is conceived (e.g. living area or total area), and the unit of calculation (m^2 or m^3, see e.g. Papathoma-Köhle et al. (2015), Röthlisberger et al. 2018).

A sensitivity analysis can show how the differences in data may influence the results and consequently the reliability of the method. In the following sections, data from multiple sources and differences in the interpretation of photographic documentation to assess the process intensity are used as a basis for the sensitivity analysis.

In more detail, the process intensity has been captured in two different ways: (a) as maximum intensity, meaning the maximum flow height that can be observed on the building envelope and (b) as mean intensity, meaning the average intensity that can be observed on the building when we consider all the sides. Moreover, the degree of loss has been calculated based on two different reconstruction value prices. The first one is an approach by Kranewitter (2017) providing averaged price levels for different building categories, and the second one is a local approach using specific costs and price levels for each case study considered.

2.4. Case studies and data collection

The Beta model and the PVI were developed based on damage data from dynamic flooding events in Austria and Italy. To test the predictive capacity of the methods, two case studies have been chosen where recently dynamic flooding events have occurred. The two case studies were Dimaro (2018, Trento, Italy) and Schallerbach (2015, Tyrol, Austria)

2.4.1. The Rotian river event and the damages in Dimaro (29 October 2018, Trento, Italy)

Dimaro is a small mountain village, located in the autonomous province of Trento, in the eastern Italian Alps (Fig. 3). The village covers an area of approximately 36.53 km^2 and the average altitude is 766 m asl (Comune di Dimaro Folgarida, 2016). According to the Italian National Institute of Statistics (ISTAT) the municipality counts 2071 inhabitants (ISTAT, 2021). The village is located on the alluvial fan of the Rotian river basin, with a drainage area of 253 km^2 and an altitude ranging between 829 and 2070 m asl.

During the last 150 years, the area has been affected by several torrential events, with two disastrous events occurring in 1882 and 1885. After the events, a system of river dykes was built to prevent the inundation of the alluvial fan. In the period 1973–1980 the first

Fig. 2. Damaged buildings in Schallerbach (Tyrol, Austria). The building is located on the slope and, for this reason the deposit height is very high at the back side of the building in comparison with the deposit height observed in the opposite side. (Source: Austrian Service for Torrent and Avalanche Control, with permission).

Fig. 3. Location of the two case studies (Basemap: Stamen Watercolor).

protection structures were planned in the headwater catchment and a system of 16 large reinforced concrete check dams was built, together with retention basins. Later, in the period 2014–2018, an open check dam was realised in the last reach of the river creek before the alluvial fan.

The extreme precipitation event occurring on 27–29 October 2018 triggered a sequence of three debris flows. With 350 mm in 72 h, the precipitation event is characterised by a return period (computed based on the technique illustrated by Norbiato et al, 2007) exceeding 300 years. In total, more than 150,000 m^3 of debris were deposited by the debris flows over the alluvial fan (Comune di Dimaro Folgarida, 2020). The deposition zone of the debris flow encountered the western part of the settled area of Dimaro, causing considerable damage to the present built environment. A woman got trapped in her home by the debris and lost her life, and 26 buildings were damaged at various degrees. About 200 people were forced to evacuate their homes (Comune di Dimaro Folgarida, 2020).

For the present study, 24 residential buildings that have suffered damage during the Dimaro event in 2018 have been identified and analysed. To assess the deposition heights a significant amount of information has been collected including (i) photographs taken only a short time after the event (ii) images from Google Street View (iii) supplemented with pictures available online from local newspapers and (iv) also videos taken by private persons found on the video-sharing platform "YouTube".

By using the set inventory of images, the deposition height is derived from the evaluation of the height of the marks left by the debris and/or the water on the walls of the structures. This process depends on the subjective perception of the data collector. To minimise a possible bias, already known heights were used for comparison. For instance, the average height of a storey in the province of Trento adds up to 2.90 m, including the height of a room with 2.60 m and the thickness of the ceiling with 0.30 m. This value can serve as a relevant reference point, as well as the average height of the lower edge of windows with approximately 1.00 m or the mean height of balcony doors with 2.00 m. The deposition heights for the 24 buildings have been estimated in two different ways: as the maximum deposition height (H_{max}) and as the average deposition height ($H_{average}$), calculated from the maximum and minimum observed deposition height.

The monetary damage to each building has been assessed for every structure individually. The reconstruction value of the building implies the repairing costs to rebuild or substitute the entire building and has been calculated by using given local standard prices in €/m^2 or €/m^3. Two different locally-linked pricing methods have been applied:

Pricing method A: The minimal real estate price for residential buildings was used, for normal maintenance status, given by the "agenzia delle entrate", the Real Estate Observatory of the Italian Revenue Agency, for the location of Dimaro in €/m^2 (gross area) for the year 2019. The resulting building value was 1700 €/m^2.

Pricing method B: The standard costs for buildings in Tyrol, Austria were used, calculated after Kranewitter (2017) in €/m^2 (net area). The resulting building value was 1650 €/m^2.

Building specific results of all calculation methods for the process intensity and the degree of loss are provided in Appendix A and are used for the sensitivity analysis.

2.4.2. The Schallerbach torrent event and the damages in Gries (08 June 2015, Tyrol, Austria)

The case study area belongs administratively to the municipality of See which is situated in the Paznaun valley in the Austrian province of Tyrol in the Eastern European Alps and, according to Statistik Austria (2019), has 1197 inhabitants.

The river Trisanna flows through the Paznaun valley, draining it into the river Inn. One of its tributaries in See is the torrent Schallerbach. The catchment of Schallerbach has a size of 8.3 km^2 and the elevation within the fan ranges from 1012 to 2936 m asl. On its flow length of 4.6 km the torrent has an average slope of approx. 28 %. The steepest part, with an average slope of 50 %, is located right above the settlement (Hübl et al., 2016).

The study area has been affected by several torrential events in the past. Past events in 1834, 1876, 1868, 1919, and 1960 caused damage to farmlands, small roads, or bridges. In 1961, the authorities started to build the first river engineering structures at the Schallerbach and constructed a channel bed and a log dam with a bedload retention basin in 1961. Earth dams secured by large boulders were also created to connect the concrete structures laterally with the terrain (Hübl et al., 2016).

On 8 June 2015, due to heavy rainfall, a debris flow occurred directing the subsequent flow over the left earth dam leading to its collapse. Consequently, about 90 % of the discharge went down the alluvial cone into the direction of the settlement. Due to the collapsed earth dam, the deposited sediments started to erode, and three waves of fluvial sediment transport hit buildings in Gries and Elis leading to severe destruction. The process was estimated to have a discharge of around 60 to 90 m^3/s and a flow speed of 4 to 6 m/s (Hübl et al., 2016). The deposition occurred mainly on the deposition cone due to the flat terrain and the retention basin. Altogether around 60,000 m^3 of sediments were deposited there; 35,000 m^3 of which were stored in the retention basin.

The debris flow, the fluvial sediment transport, and erosion resulting from the torrential event caused damage to infrastructure as well as to buildings. Several small roads were destroyed and federal road B 188 was temporarily closed. According to the event documentation (Hübl et al., 2016), 70 houses were damaged and four were completely destroyed. However, a recent report claims that 45 houses were damaged whereas the damage protocols list 32 houses that suffered loss (Kurz and Jäger, 2019). The reported damage acknowledged by appraisers for private houses ins Gries and Elis (cars excluded) summed up to 6.21 million € (for the 32 buildings).

For the present study, 21 buildings in the district of Gries that have suffered damage during the Schallerbach event in 2015 have been identified and analysed. The affected buildings were either residential buildings or hotels. In this study, however, only residential buildings were considered. Most of them were constructed with brick masonry and the majority of the houses (16 out of 21) were constructed after 1970. The buildings were rather big for single-family houses, with a mean gross area of 454 m^2 per building.

In the damage protocols, there are 33 entries of damage data from houses of the study area, however, only 21 of those are used in this study because only for these buildings the required data were available.

The degree of loss was calculated using two different pricing methods:

Pricing method A: The standard costs for buildings in Tyrol, Austria were used, calculated after Kranewitter (2017) in €/m^2 (net area). The resulting building value was 1650 €/m^2.

Pricing method B: Reconstruction values were calculated based on the building volume and interpolation, the resulting value was 540 €/m^3.

In more detail, pricing method A provided average prices for construction costs for different building types and standards. These prices are given in € per gross square meter and for a room height of 2.8 m. Furthermore, it was possible to calculate the values for areas of different usage by multiplying the adapted value with different reduction factors following ranges given in Kranewitter (2017), which were 40 % to 70 % of the adapted value (for cellars, garages, and side buildings) and 70 % to 100 % of the adapted value (for attics). The pricing method B used for the calculation was based on the building volume which was calculated based on digital elevation models. A digital model of difference was calculated by subtracting the surface model (DSM) from the terrain model (DTM) (DSM 2012 – DTM 2012). The result was a model with the height of all filtered parts, such as buildings or trees. Then the sum of all pixel values in the shapes of the buildings of the digital cadastral map

was calculated. This value provided an approximation for the building volume. Next, the building volumes were multiplied by a price variable of € 540 per cubic meter of building volume, which equaled the reconstruction value.

The buildings were affected by maximum deposition heights ranging from 0.1 m to 3.4 m. The hazard intensity was assessed in two different ways by taking the maximum deposition height (H_{max}) and the mean upslope deposition height (H_{upmean}) for each building into account.

The maximum and mean intensity as well as the degree of loss per building calculated in two different ways for the Schallerbach case study are shown in Appendix B.

3. Results

3.1. Application of the Beta model

The data from the two case studies are displayed together with data used in the original Beta model (Fuchs et al., 2019a) in Fig. 4.

It becomes obvious that the overall degree of loss is below a range of around 0.4 for all intensity values in both of the case studies. Similarly, the increase of the vulnerability curve with increasing process intensities cannot be observed as clearly as in the original Beta model. Although for low process intensities the data points are located close to the curve of the original Beta model, for intensities higher than 2 m the degree of loss ranges between 0.05 and 0.4 with one exception. If the data of both of the case studies are regarded in relation to the original shape of the model, considerable differences become evident (Fig. 5). For both of the case studies process intensities higher than 1 m result in an underestimation of the original model (Fig. 5, upper and lower left), with a maximum around intensities of 2.5 m. If the calculation is computed with mean process intensities, the deviation is naturally less obvious because data get shifted to the left on the x-axis, with the same value of the degree of loss on the y-axis (Fig. 5, upper and lower right). However, for the Dimaro case study an underestimation of around 10 % is still detectable for process intensities higher than 1 m. This provides evidence on the importance of the process intensity as an explaining variable. In contrast, the use of different methods to determine the degree of loss seems to have less influence on the results (Fig. 5, upper and lower row).

An explanation for these results may be associated with the design and architectural characteristics of the buildings or the surroundings due to architectural or structural particularities that are not considered in the Beta model. These particularities may include differences in the material and design of buildings, surroundings that may offer protection (walls, vegetation), or even particularities such as balconies or other protruding parts. Instead, the Beta model mirrors the average vulnerability which has been empirically derived from the underlying case studies. It is, therefore, crucial to include such information when we assess the physical vulnerability of the buildings. Hence, the vulnerability index could be a promising approach, and the index can be used to supplement loss information given by (empirical) vulnerability curves.

3.2. Application and sensitivity analysis of the PVI

3.2.1. Application in Dimaro

According to equation (1), the physical vulnerability index was calculated for the 24 reviewed buildings with the subsequent results. The spatial distribution of the PVI is shown in Fig. 6. The PVI per building is shown in Appendix A.

The validation of the PVI in Dimaro is based on the comparison between the PVI of the buildings and the observed degree of loss during the 2018 event. From the distribution of the PVI it becomes evident that there is a cluster of buildings with high PVI in the east part of the village. Buildings with lower PVI are mostly located in the lower part of the valley, and buildings with higher PVI are located in proximity to depositions of the 2018 event. Nevertheless, some buildings located on higher ground close to the forest have a low PVI (blue colour) because they may also be protected by the vegetation around them. In the highly-exposed cluster of buildings, a building with lower PVI (orange colour) is surrounded and probably also protected by some buildings with higher PVI (red colour). Such so-called shielding effects of buildings to neighbouring structures in mountain areas have been also recently reported from laboratory studies by Sturm et al. (2018a, b).

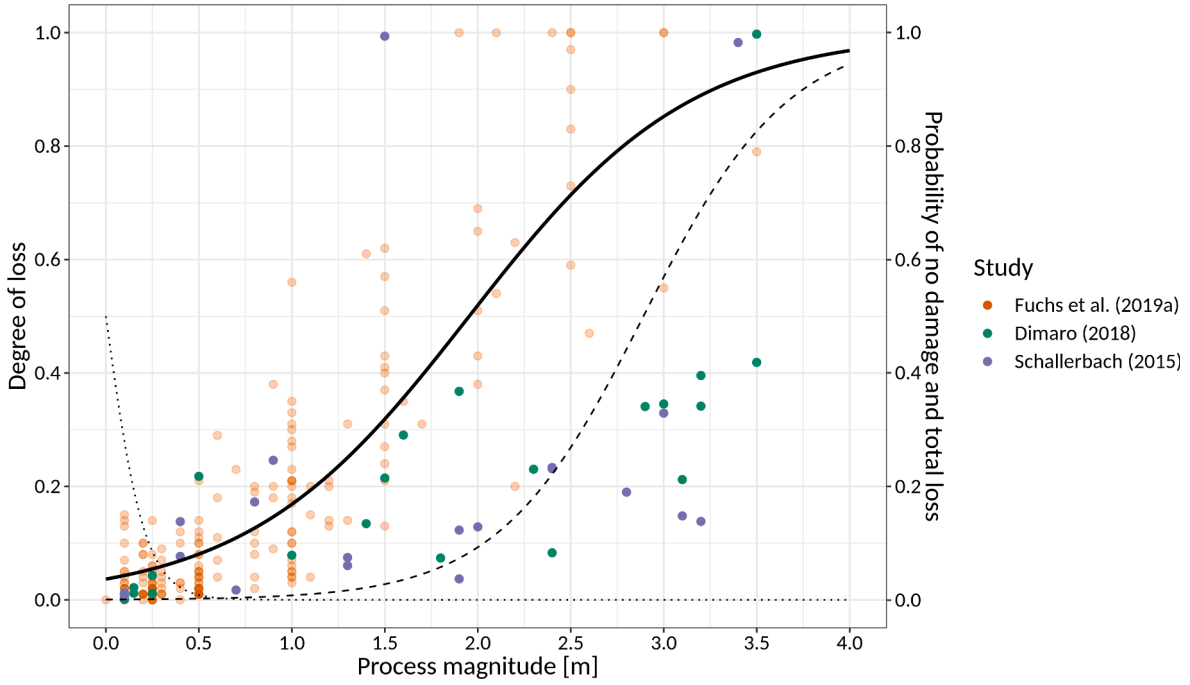

Fig. 4. The data used in the original Beta model (orange) (Fuchs et al., 2019a), supplemented by data from the case studies (green and blue). The solid black line shows the mean damage of the underlying Beta distribution as a result of different intensities (deposit height). The dotted line shows the probability of an undamaged building, and the dashed line shows the probability of a building being completely destroyed.

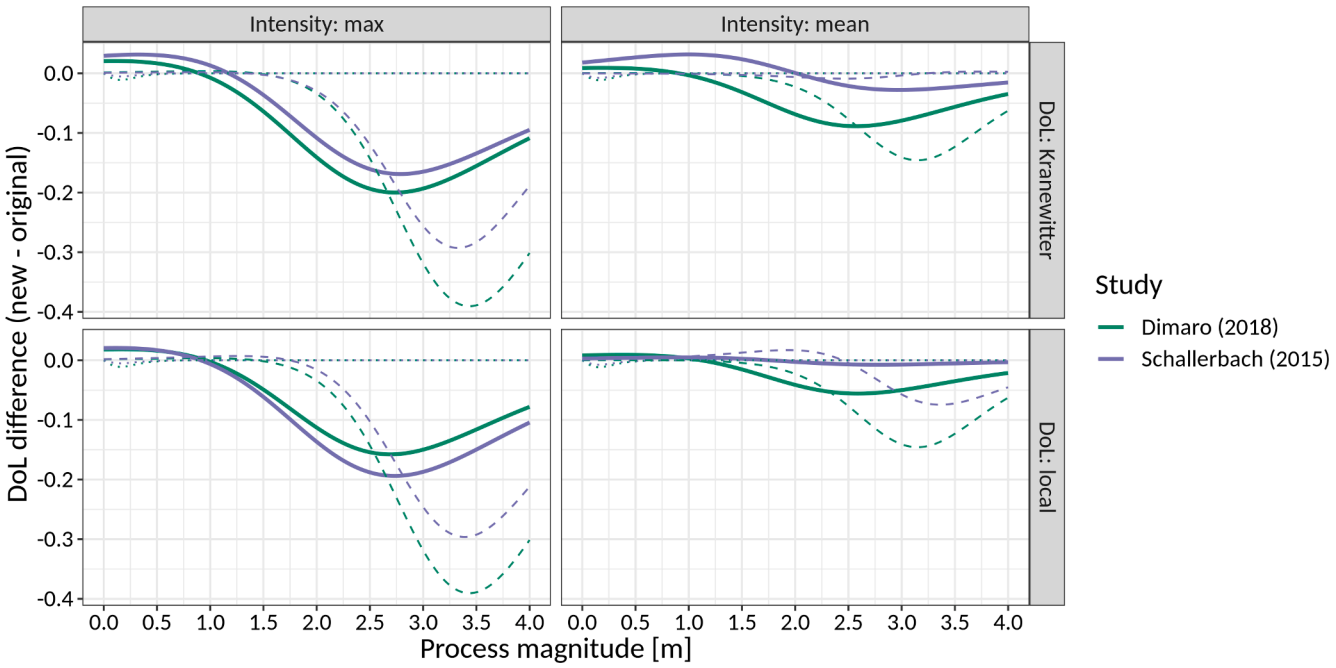

Fig. 5. Figure shows the difference between the original Beta model (vulnerability curve) and the vulnerability relation for the case studies of Dimaro and Schallerbach. The solid lines indicate the difference in mean damage of the underlying Beta distribution as a result of different process intensities (deposit height). The dashed lines show the difference in probability of an undamaged building, and the dotted lines show the difference in the probability of a building being completely destroyed.

Fig. 6. Spatial distribution of the PVI (four vulnerability classes: very low (blue), low (light blue), high (orange), and very high (red)) in Dimaro.

3.2.2. *Application in Schallerbach*

The PVI has been also calculated for all the 21 damaged buildings in Schallerbach and its spatial distribution is shown in Fig. 7. The PVI for each building is given in Appendix B.

The spatial distribution of the PVI shows that there is a cluster of highly vulnerable buildings (red colour) in the centre of the case study area. Nevertheless, buildings that had direct contact with the flowing water body belong to the second-highest vulnerability class (orange colour). Similar to the Dimaro case study, shielding effects resulting from a protective function of buildings closer to the process area can be observed, and buildings that belong to the two lowest PVI classes seem to be protected by a cluster of buildings that are located on higher ground behind them.

3.2.3. *Validation and sensitivity analysis*

The relationship between the PVI and the degree of loss is demonstrated in Fig. 8 by four panels. The left panels show the PVI for the maximum process intensity and the right panels show the PVI for the mean intensity. In all plots, it becomes evident that buildings that have experienced a low degree of loss have been also assigned a very low PVI.

Fig. 7. Spatial distribution of the PVI (four vulnerability classes very low (blue), low (light blue), high (orange) and very high (red)) in Schallerbach.

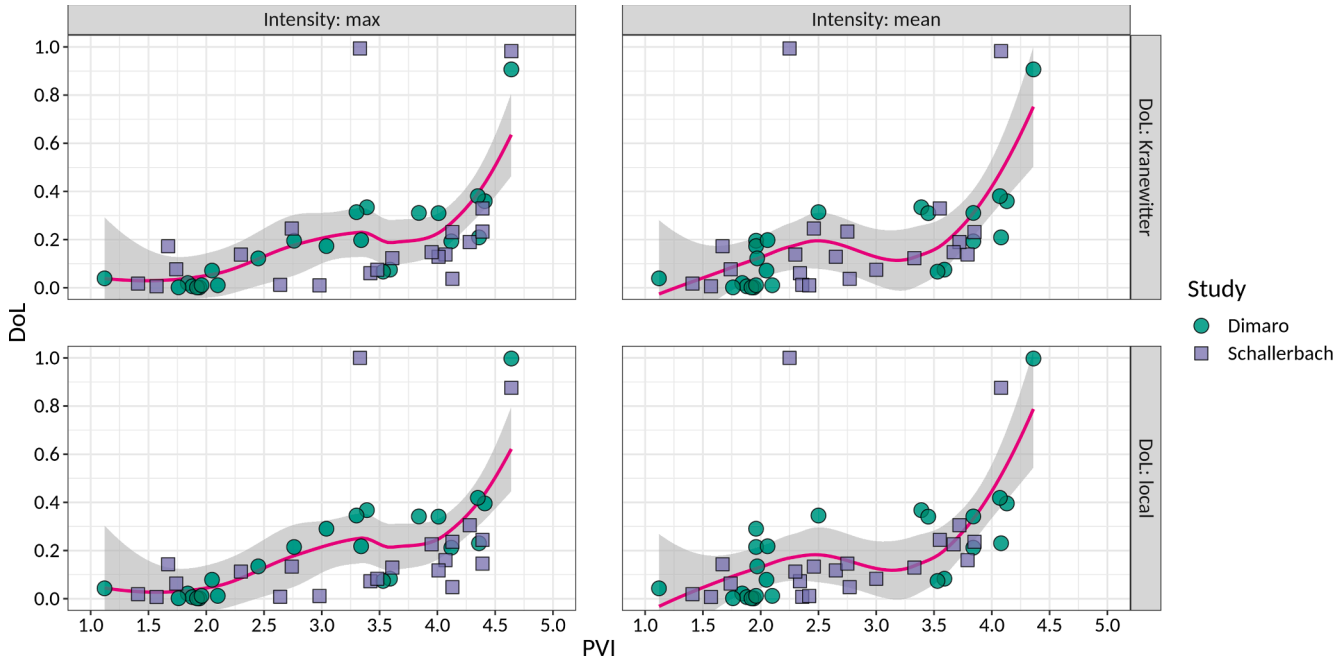

Fig. 8. Panels showing the PVI calculated considering maximum (left) and mean (right) intensity and local degree of loss (lower) or degree of loss (DoL) calculated after Kranewitter (2017) (upper).

In turn, with an increasing PVI the degree of loss is also increasing in all four panels, which is consistent with the overall expectation. Similar to the vulnerability curves, the key variable here is the process intensity, which is also mirrored in equation (1) accordingly by a high weighting factor. Moreover, the insignificant influence of different methods to calculate the degree of loss on the overall result is evident.

Even though the PVI includes some information on building characteristics, which renders it a useful method to complement vulnerability curves (which rely on process intensity only), some unobserved heterogeneities remain. In Fig. 9, two buildings in Schallerbach are shown that represent both a degree of loss of almost 1 (violet squares in Fig. 8). These show different PVI values of 3.3 and 4.6, respectively, if the maximum process intensity is considered. Hence, information other than those considered during the calculation of the PVI (e.g. material of construction, number of floors, wall thickness) may also be important to gain full insight into the physical vulnerability of buildings exposed.

From all these observations it can be assumed that when the maximum process intensity is considered, the PVI performs better than when the mean intensity is considered, which is in line with the fact that the original weighting was established using maximum process intensity as a basis. However, as far as the degree of loss is considered, the differences are minimal.

Fig. 9. Two buildings that experienced the highest degree of loss (approximately 1) in the Schallerbach case study (Source: WLV).

4. Discussion and conclusion

For the assessment of physical vulnerability, two different methods have been applied to two case studies: vulnerability curves and vulnerability indicators. The first (Beta model) turned out to overestimate the losses in comparison to similar events that occurred in the past (e.g., Fuchs et al., 2019a). It is clear from Fig. 4 that the data from Dimaro and Schalerbach (blue and green dots) lie significantly lower than the data from past events (orange dots) This may be attributed to local differences in the housing which reflects on of the main disadvantages of vulnerability curves which is the lack of consideration of the characteristics of the buildings. The application of the second approach (PVI) showed that it may be used to complement the use of vulnerability curves and provide insights on local-scale damage patterns (e.g., Papathoma-Köhle et al., 2019).

For the present study, a number of assumptions and limitations have to be pointed out. The expression of the process intensity only by using one property (deposit height) of the process is one of the limitations of the study. Moreover, detailed damage data are not always available partly due to the lack of standardised processes for their collection but also due to time limitations (building owners start cleaning and repair damages right after the event). Finally, the amount of available data is still relatively low but with ongoing updating of the database, an improvement of the tools and their reliability can be expected.

However, an overall consistency of both methods has been demonstrated, leading to the conclusion that vulnerability indices such as the PVI can be used to supplement vulnerability curves during the assessment of vulnerability. There was strong evidence in both methods applied that accurate and consistent information on process intensity is a key variable for the assessment of vulnerability, whereas differences in the calculation of building values are less important. The overall range in the data, however, is a result of many factors; some of them have not been identified in the damage and event documentation underlying the presented case studies. Consequently, to avoid such unobserved heterogeneities, there is a strong need to expand the information collected so that the explanatory power of both, vulnerability curves and indices can be enhanced. Specifically, we propose the collection of additional information during event and loss documentation. Such information may include indicators related to the design and architecture of buildings (Holub et al., 2012; Schinke et al., 2016), the building material and state of maintenance (Neubert et al., 2016), available retrofitting and local structural protection (Attems et al., 2020; Rehan, 2018), as well as other information on loss characteristics (Zischg et al., 2021). In this way, it is possible to update the vulnerability index but also to include local characteristics should the study area not share similar architecture with the areas used for the development of the index.

It has also been shown that data regarding building characteristics may be collected either through fieldwork or by using photographic documentation or even online tools such as Google Street Map, which in turn makes this method also suitable for application in data-scarce regions (Malgwi et al., 2020). The majority of the required data is straightforward (e.g. orientation of the building, building surroundings, etc.) but some of them are related to the expected processes intensity and need therefore careful evaluation (e.g. height of openings).

To conclude, indicator-based methods for the assessment of physical vulnerability are on the rise and can act as a good alternative to the use of vulnerability curves. The application showed the reliability of the method and a sensitivity analysis provided valuable support for improved event documentation. In more detail, according to the results, the way the reconstruction value of a building is calculated may be flexible, whereas it is obvious that the consideration of the highest intensity of the process leads to more reliable results. Finally, the consideration of additional indicators may be necessary, but this requires additional data from buildings that have suffered damage from dynamic flooding. Tools such as the vulnerability curves and the vulnerability index should be continuously updated and improved since they provide quantitative information regarding the possible loss of future events.

CRediT authorship contribution statement

Maria Papathoma-Köhle: Conceptualization, Methodology, Writing – original draft, Writing – review & editing, Supervision, Project administration, Funding acquisition. **Matthias Schlögl:** Data curation, Visualization, Software, Formal analysis. **Lea Dosser:** Investigation, Formal analysis. **Florian Roesch:** Investigation, Formal analysis. **Marco Borga:** Writing – review & editing. **Marcel Erlicher:** Investigation. **Margreth Keiler:** Writing – review & editing. **Sven Fuchs:** Conceptualization, Methodology, Writing – original draft, Writing – review & editing, Resources, Supervision.

Declaration of Competing Interest

The authors declare that they have no known competing financial interests or personal relationships that could have appeared to influence the work reported in this paper.

Acknowledgment

Maria Papathoma-Köhle has been supported by the Austrian Science Fund (FWF): V-519-N29.

Appendix A. Supplementary data

Supplementary data to this article can be found online at https://doi.org/10.1016/j.jhydrol.2022.127501.

References

Agliata, R., Bortone, A., Mollo, L., 2021. Indicator-based approach for the assessment of intrinsic physical vulnerability of the built environment to hydro-meteorological

hazards: review of indicators and example of parameters selection for a sample area. Int. J. Disaster Risk Reduct. 58, 102199. https://doi.org/10.1016/j.ijdrr.2021.102199.
Arrighi, C., Mazzanti, B., Pistone, F., Castelli, F., 2020. Empirical flash flood vulnerability functions for residential buildings. Springer Nat. Appl. Sci. 2 (4) https://doi.org/10.1007/s42452-020-2696-1.
Attems, M.-S., Thaler, T., Genovese, E., Fuchs, S., 2020. Implementation of property level flood risk adaptation (PLFRA) measures: choices and decisions. WIREs. Water 7 (1). https://doi.org/10.1002/wat2.1404.
Borga, M., Stoffel, M., Marchi, L., Marra, F., Jakob, M., 2014. Hydrogeomorphic response to extreme rainfall in headwater systems: flash floods and debris flows. J. Hydrol. 518, 194–205. https://doi.org/10.1016/j.jhydrol.2014.05.022.
Cammerer, H., Thieken, A., Lammel, J., 2013. Adaptability and transferability of flood loss functions in residential areas. Nat. Hazards Earth Syst. Sci. 13 (11), 3063–3081. https://doi.org/10.5194/nhess-13-3063-2013.
Cappabianca, F., Barbolini, M., Natale, L., 2008. Snow avalanche risk assessment and mapping: a new method based on a combination of statistical analysis, avalanche dynamics simulation, and empirically-based vulnerability relations integrated in a GIS platform. Cold Reg. Sci. Technol. 54 (3), 193–205. https://doi.org/10.1016/j.coldregions.2008.06.005.
Church, M., Jakob, M., 2020. What Is a debris flood? Water Resources Research, 56(8): e2020WR027144. 10.1029/2020wr027144.
Chow, C., Andrášik, R., Fischer, B., Keiler, M., 2019. Application of statistical techniques to proportional loss data: evaluating the predictive accuracy of physical vulnerability to hazardous hydro-meteorological events. J. Environ. Manage. 246, 85–100. https://doi.org/10.1016/j.jenvman.2019.05.084.
Chow, C., Ramirez, J., Keiler, M., 2018. Application of sensitivity analysis for process model calibration of natural hazards. Geosciences 8 (6), 218. https://doi.org/10.3390/geosciences8060218.
Comune di Dimaro Folgarida, 2016. Dimaro [Online]. Available at [Accessed 01/09/2021].
Comune di Dimaro Folgarida, 2020. Dimaro [Online]. Available at http://dimarovive.it/ [Accessed 01/09/2021].
Cutter, S., Finch, C., 2008. Temporal and spatial changes in social vulnerability to natural hazards. PNAS 105 (7), 2301–2306. https://doi.org/10.1073/pnas.0710375105.
Englhardt, J., de Moel, H., Huyck, C.K., de Ruiter, M.C., Aerts, J.C., Ward, P.J., 2019. Enhancement of large-scale flood risk assessments using building-material-based vulnerability curves for an object-based approach in urban and rural areas. Nat. Hazards Earth Syst. Sci. 19 (8), 1703–1722. https://doi.org/10.5194/nhess-19-1703-2019.
Fekete, A., 2019. Social vulnerability (re-)assessment in context to natural hazards: Review of the usefulness of the spatial indicator approach and investigations of validation demands. Int. J. Disaster Risk Sci. 10 (2), 220–232. https://doi.org/10.1007/s13753-019-0213-1.
Fuchs, S., Heiser, M., Schlögl, M., Zischg, A., Papathoma-Köhle, M., Keiler, M., 2019a. Short communication: a model to predict flood loss in mountain areas. Environ. Modell. Software 117, 176–180. https://doi.org/10.1016/j.envsoft.2019.03.026.
Fuchs, S., Heiss, K., Hübl, J., 2007. Towards an empirical vulnerability function for use in debris flow risk assessment. Nat. Hazards Earth Syst. Sci. 7 (5), 495–506. https://doi.org/10.5194/nhess-7-495-2007.
Fuchs, S., Keiler, M., Ortlepp, R., Schinke, R., Papathoma-Köhle, M., 2019b. Recent advances in vulnerability assessment for the built environment exposed to torrential hazards: challenges and the way forward. J. Hydrol. 575, 587–595. https://doi.org/10.1016/j.jhydrol.2019.05.067.
Fuchs, S., Keiler, M., Zischg, A., 2015. A spatiotemporal multi-hazard exposure assessment based on property data. Nat. Hazards Earth Syst. Sci. 15 (9), 2127–2142. https://doi.org/10.5194/nhess-15-2127-2015.
Fuchs, S., McAlpin, M.C., 2005. The net benefit of public expenditures on avalanche defense structures in the municipality of Davos, Switzerland. Nat. Hazards Earth Syst. Sci. 5 (3), 319–330. https://doi.org/10.5194/nhess-5-319-2005.
Gall, M., Borden, K., Cutter, S., 2009. When do losses count? six fallacies of natural hazards loss data. Bull. Am. Meteorol. Soc. 90 (6), 799–809. https://doi.org/10.1175/2008BAMS2721.1.
Holub, M., Fuchs, S., 2009. Mitigating mountain hazards in Austria – Legislation, risk transfer, and awareness building. Nat. Hazards Earth Syst. Sci. 9 (2), 523–537. https://doi.org/10.5194/nhess-9-523-2009.
Holub, M., Suda, J., Fuchs, S., 2012. Mountain hazards: reducing vulnerability by adapted building design. Environ. Earth Sci. 66 (7), 1853–1870. https://doi.org/10.1007/s12665-011-1410-4.
Hübl, J., Beck, M., Zöchling, M., Moser, M., Kienberger, C., Jenner, A., Forstlechner, D., 2016. Ereignisdokumentation 2015. IAN Report 175. Universität für Bodenkultur, Institut für alpine Naturgefahren, Wien, 124 pp.
ISTAT, 2021. Population and households [Online]. Available at https://dati.istat.it/Index.aspx?QueryId=19101&lang=en [Accessed 01/09/2021].
Jakob, M., Stein, D., Ulmi, M., 2012. Vulnerability of buildings to debris flow impact. Nat. Hazards 60 (2), 241–261. https://doi.org/10.1007/s11069-011-0007-2.
Karagiorgos, K., Thaler, T., Heiser, M., Hübl, J., Fuchs, S., 2016. Integrated flash flood vulnerability assessment: insights from East Attica, Greece. J. Hydrol. 541, 553–562. https://doi.org/10.1016/j.jhydrol.2016.02.052.
Kranewitter, H., 2017. Liegenschaftsbewertung. Manz, Wien, p. 390.
Kurz, D., Jäger, G., 2019. Aufwendige Projektierung unter Einbeziehen der Bevölkerung nach einem Katastrophenereignis am Schallerbach in Tirol/Österreich. Dresdner Wasserbauliche Mitteilungen 62, 251–261.
Malgwi, M.B., Fuchs, S., Keiler, M., 2020. A generic physical vulnerability model for floods: review and concept for data-scarce regions. Nat. Hazards Earth Syst. Sci. 20 (7), 2067–2090. https://doi.org/10.5194/nhess-20-2067-2020.
Malgwi, M.B., Schlögl, M., Keiler, M., 2021. Expert-based versus data-driven flood damage models: A comparative evaluation for data-scarce regions. Int. J. Disaster Risk Reduct. 57, 102148 https://doi.org/10.1016/j.ijdrr.2021.102148.
Mazzorana, B., Comiti, F., Fuchs, S., 2013. A structured approach to enhance flood hazard assessment in mountain streams. Nat. Hazards 67 (3), 991–1009. https://doi.org/10.1007/s11069-011-9811-y.
Mazzorana, B., Comiti, F., Scherer, C., Fuchs, S., 2012. Developing consistent scenarios to assess flood hazards in mountain streams. J. Environ. Manage. 94 (1), 112–124. https://doi.org/10.1016/j.jenvman.2011.06.030.
Mazzorana, B., Simoni, S., Scherer, C., Gems, B., Fuchs, S., Keiler, M., 2014. A physical approach on flood risk vulnerability of buildings. Hydrol. Earth Syst. Sci. 18 (9), 3817–3836. https://doi.org/10.5194/hess-18-3817-2014.
Milanesi, L., Pilotti, M., Bacchi, B., 2016. Using web-based observations to identify thresholds of a person's stability in a flow. Water Resour. Res. 52 (10), 7793–7805. https://doi.org/10.1002/2016WR019182.
Milanesi, L., Pilotti, M., Belleri, A., Marini, A., Fuchs, S., 2018. Vulnerability to flash floods: A simplified structural model for masonry buildings. Water Resour. Res. 54 (10), 7177–7197. https://doi.org/10.1029/2018WR022577.
Moreira, L.L., de Brito, M.M., Kobiyama, M., 2021. Effects of different normalization, aggregation, and classification methods on the construction of flood vulnerability indexes. Water 13 (1), 98. https://doi.org/10.3390/w13010098.
Neubert, M., Naumann, T., Hennersdorf, J., Nikolowski, J., 2016. The Geographic Information System-based flood damage simulation model HOWAD. J. Flood Risk Manage. 9 (1), 36–49. https://doi.org/10.1111/jfr3.12109.
Norbiato, D., Borga, M., Sangati, M., Zanon, F., 2007. Regional frequency analysis of extreme precipitation in the eastern Italian Alps and the August 29, 2003 flash flood. J. Hydrol. 345 (3–4), 149–166. https://doi.org/10.1016/J.JHYDROL.2007.07.009.
Papathoma-Köhle, M., Gems, B., Sturm, M., Fuchs, S., 2017. Matrices, curves, and indicators: a review of approaches to assess physical vulnerability to debris flows. Earth Sci. Rev. 171, 272–288. https://doi.org/10.1016/j.earscirev.2017.06.007.
Papathoma-Köhle, M., Keiler, M., Totschnig, R., Glade, T., 2012. Improvement of vulnerability curves using data from extreme events: debris flow event in South Tyrol. Nat. Hazards 64 (3), 2083–2105. https://doi.org/10.1007/s11069-012-0105-9.
Papathoma-Köhle, M., Schlögl, M., Fuchs, S., 2019. Vulnerability indicators for natural hazards: an innovative selection and weighting approach. Scientific Reports, 9: Article 15026. 10.1038/s41598-019-50257-2.
Papathoma-Köhle, M., Zischg, A., Fuchs, S., Glade, T., Keiler, M., 2015. Loss estimation for landslides in mountain areas - An integrated toolbox for vulnerability assessment and damage documentation. Environ. Modell. Software 63, 156–169. https://doi.org/10.1016/j.envsoft.2014.10.003.
Papathoma-Köhle, M. 2016. Vulnerability curves vs. vulnerability indicators: application of an indicator-based methodology for debris-flow hazards. Natural Hazards and Earth System Science, 16, 1771-1790. 10.5194/nhess-16-1771-2016.
Quan Luna, B., Blahut, J., van Westen, C.J., Sterlacchini, S., van Asch, T.W.J., Akbas, S. O., 2011. The application of numerical debris flow modelling for the generation of physical vulnerability curves. Nat. Hazards Earth Syst. Sci. 11 (7), 2047–2060. https://doi.org/10.5194/nhess-11-2047-2011.
Rehan, B.M., 2018. Accounting public and individual flood protection measures in damage assessment: A novel approach for quantitative assessment of vulnerability and flood risk associated with local engineering adaptation options. J. Hydrol. 563, 863–873. https://doi.org/10.1016/j.jhydrol.2018.06.061.
Röthlisberger, V., Zischg, A.P., Keiler, M., 2018. A comparison of building value models for flood risk analysis. Nat. Hazards Earth Syst. Sci. 18 (9), 2431–2453. https://doi.org/10.5194/nhess-18-2431-2018.
Schinke, R., Kaidel, A., Golz, S., Naumann, T., Lopez-Gutierrez, J.S., Garvin, S., 2016. Analysing the effects of flood-resilience technologies in urban areas using a synthetic model approach. Int. J. Geo-Infor. 5 (11), 202. https://doi.org/10.3390/ijgi5110202.
Schlögl, M., Richter, G., Avian, M., Thaler, T., Heiss, G., Lenz, G., Fuchs, S., 2019. On the nexus between landslide susceptibility and transport infrastructure – an agent-based approach. Nat. Hazards Earth Syst. Sci. 19 (1), 201–219. https://doi.org/10.5194/nhess-19-201-2019.
Slaymaker, O., 2010. Mountain Hazards. In: Alcantara-Ayala, I. (Ed.), Geomorphological Hazards and Disaster Prevention. Cambridge University Press, Cambridge, pp. 33–48.
Statistik Austria, 2019. STATatlas [Online]. Available at www.statistik.at/atlas/ [Accessed 10 January 2020.
Sturm, M., Gems, B., Keller, F., Mazzorana, B., Fuchs, S., Papathoma-Köhle, M., Aufleger, M., 2018a. Experimental analyses of impact forces on buildings exposed to fluvial hazards. J. Hydrol. 565, 1–13. https://doi.org/10.1016/j.jhydrol.2018.07.070.
Sturm, M., Gems, B., Keller, F., Mazzorana, B., Fuchs, S., Papathoma-Köhle, M., Aufleger, M., 2018b. Understanding the dynamics of impacts at buildings caused by fluviatile sediment transport processes. Geomorphology 321, 45–59. https://doi.org/10.1016/j.geomorph.2018.08.016.
Thaler, T., Zischg, A., Keiler, M., Fuchs, S., 2018. Allocation of risk and benefits – distributional justices in mountain hazard management. Reg. Environ. Change 18 (2), 353–365. https://doi.org/10.1007/s10113-017-1229-y.
Totschnig, R., Fuchs, S., 2013. Mountain torrents: quantifying vulnerability and assessing uncertainties. Eng. Geol. 155, 31–44. https://doi.org/10.1016/j.enggeo.2012.12.019.
Totschnig, R., Sedlacek, W., Fuchs, S., 2011. A quantitative vulnerability function for fluvial sediment transport. Nat. Hazards 58 (2), 681–703. https://doi.org/10.1007/s11069-010-9623-5.

Vamvatsikos, D., Kouris, L. A., Panagopoulos, G., Kappos, A. J., Nigro, E., Rosetto, T., Lloyd, T. O. & Stathopoulos, T. 2010. Structural vulnerability assessment under natural hazards: a review. In: MAZZOLANI, ed. Urban Habitat Constructions under Catastrophic Events, 2010. Taylor & Francis Group, 711-722.

Zhang, S., Zhang, L., Li, X., Xu, Q., 2018. Physical vulnerability models for assessing building damage by debris flows. Eng. Geol. 247, 145–158. https://doi.org/10.1016/j.enggeo.2018.10.017.

Zischg, A., Hofer, P., Mosimann, M., Röthlisberger, V., Ramirez, J.A., Keiler, M., Weingartner, R., 2018. Flood risk (d)evolution: disentangling key drivers of flood risk change with a retro-model experiment. Sci. Total Environ. 639, 195–207. https://doi.org/10.1016/j.scitotenv.2018.05.056.

Zischg, A.P., Röthlisberger, V., Mosimann, M., Profico-Kaltenrieder, R., Bresch, D.N., Fuchs, S., Kauzlaric, M., Keiler, M., 2021. Evaluating targeted heuristics for vulnerability assessment in flood impact model chains. J. Flood Risk Manage. e12736 https://doi.org/10.1111/jfr3.12736.

Zou, Q., Cui, P., Zhou, G.D., Li, S., Tang, J., Li, S., 2018. A new approach to assessing vulnerability of mountain highways subject to debris flows in China. Prog. Phys. Geogr. 42 (3), 305–329. https://doi.org/10.1177/0309133318770985.